J. Wind Eng. Ind. Aerodyn. 144 (2015) 146–153

Contents lists available at ScienceDirect

Journal of Wind Engineering and Industrial Aerodynamics

journal homepage: www.elsevier.com/locate/jweia

The impact of stable atmospheric boundary layers on wind-turbine wakes within offshore wind farms

Martin Dörenkämper*, Björn Witha, Gerald Steinfeld, Detlev Heinemann, Martin Kühn

ForWind – Center for Wind Energy Research, Department of Physics, Carl von Ossietzky University Oldenburg, D-26129 Oldenburg, Germany

ARTICLE INFO

Keywords:
Atmospheric stratification
Boundary layer
Large-eddy simulation
Wind energy
Wind turbine wakes

ABSTRACT

In terms of predicting wind turbine wakes, the stably stratified atmospheric boundary layer (SABL) is taking an exceptional position as wake effects and thus loads on subsequent turbines are stronger. In this study we show the impact of the SABL on power production and wake effects (power deficits) in offshore wind farms by means of measurements as well as large-eddy simulations (LES). Measurements show enhanced wake effects in the SABL compared to the unstable situation. Another influence on the power generation of an offshore wind farm is the distance of the wind farm to the shore. This is accounted for in the LES by a modification of surface characteristics at the coastal discontinuity. In addition to the effect of the coast, the numerical case study also shows the existence of local jets between the turbines of the wind farm.

1. Introduction

The number of wind turbines being connected to the electrical grid worldwide is increasing rapidly. In Europe, the wind-energy capacity is expected to grow up to more than 130 GW within the next decades. Most of the projected and also the already erected offshore wind farms are located in rather small regions like the North Sea and also the Baltic Sea (EWEA, 2014). Further limitations (e.g. shipping routes and nature reserves) lead to very limited areas where hundreds of turbines will be built. Thus, inter- and intra-wind farm wake effects are an important issue for the power output of these offshore wind farms.

Due to its far extension into northern latitudes, the related cooling of the water masses in winter and its proximity to the shores, the atmospheric boundary layer (ABL) over the Baltic Sea is dominated by stable stratification. Smedman et al. (1997) found for locations on the southern Swedish coast that two-thirds of all situations were stably stratified. This is in contrast to the ABL over the North Sea which is predominantly neutrally to slightly unstably stratified (Sathe et al., 2011). The larger probability of stable atmospheric boundary layer (SABL) states also leads to an increased frequency of low-level jets (Smedman et al., 1996).

The atmospheric stability is an important meteorological variable impacting the development of wind turbine wakes in offshore wind farms. This impact has been investigated in several studies within the last years. Barthelmie et al. (2007) showed the dependence of wind speed deficits on stability for the offshore wind farm Nysted in the Baltic Sea. Hansen et al. (2012) reported a strong dependency of the power deficit inside the offshore wind farm Horns Rev on atmospheric stability. They found, based on measurements at an offshore met mast in the North Sea, that offshore stable and unstable conditions are present at wind speeds up to 15 m s^{-1}. Above this wind speed neutral conditions (very small absolute value of the Richardson-number) prevail because the shear production of turbulence dominates over the buoyancy production/consumption. In addition, they reported a dependency of the intensity and the width of wind turbine wakes on atmospheric stability inside an offshore wind farm with the largest deficits for very stable and stable conditions.

One main reason for the impact of atmospheric stability on the power output of offshore wind farms is the size of turbulent momentum fluxes in the atmosphere which act in refilling the wakes. The role of these momentum fluxes for large wind farms has been described in Emeis (2010). More recently, investigations of power data for single offshore wind turbines showed differences of up to 20% between stable and unstable stratification for the same mean wind speed (e.g. Dörenkämper et al., 2014).

The power output in the non-wake case is lower in an SABL for the same hub height wind speed of the ambient flow. Dörenkämper et al. (2014) explain this by the increase in shear in the inflow of a multi-megawatt offshore wind turbine which is not captured by a single hub height inflow measurement. The increase in shear in the lower part of the rotor disk is not compensated in the upper part of the rotor. Furthermore their study showed that low turbulence intensities also lead to a decreased power output for equal inflow wind speeds. In contrast to this study, Wharton and Lundquist

* Corresponding author. Tel.: +49 441 798 5077; fax: +49 441 798 5099.
E-mail address: martin.doerenkaemper@uni-oldenburg.de (M. Dörenkämper).

http://dx.doi.org/10.1016/j.jweia.2014.12.011

(2010) found a decreased power output for unstable conditions. They did not use a single measurement at the inflow but calculated a "true-flux" equivalent wind speed which then incorporates the impact of shear and turbulence.

Nowadays available computational power and enhanced wind turbine parametrizations allow for detailed studying of wind turbine wakes in offshore wind farms. First numerical investigations of the flow around wind turbines were mainly based on the Reynolds-averaged Navier–Stokes (RANS) solvers through single wind turbines (among others Sørensen and Shen, 2002; El Kasmi and Masson, 2008). These studies lack in resolving important turbulent quantities and a detailed structure of the wake in wind farm simulations. More recently, the development of high-performance parallel computers facilitates simulations of atmospheric turbulence-resolving large-eddy simulations (LES). First studies were limited to single wind turbines (e.g. Jimenez et al., 2007) and/or idealized inflow conditions neglecting Coriolis or buoyancy effects (e.g. Porté-Agel et al., 2011).

LES of entire wind farms in varying atmospheric stratification are currently a subject of investigation. Churchfield et al. (2012) performed a wind farm LES of the entire Lillgrund offshore wind farm with 48 wind turbines in a neutrally stratified ABL including Coriolis force and found an overprediction of relative power by 25–40% compared to field data. The power losses at the Horns Rev offshore wind farm were investigated by Porté-Agel et al. (2013) for different inflow angles in neutrally stratified flow concluding that only small changes in wind direction can have a strong influence on the total power output of the entire wind farm. Most recent studies encompass convective and stable boundary layers in LES of wind turbine wakes (e.g. Aitken et al., 2014; Mirocha et al., 2014).

The objectives of this study are to show the impact of atmospheric stability on wind turbine wakes derived from measured Supervisory Control and Data Acquisition (SCADA) data, followed by a case study of a developing SABL after a coastal passage and its impact on wind turbine wakes within an offshore wind farm.

Section 2 introduces the data and the LES framework used in this study. In Section 3 measured wake effects are presented first before they are further investigated in the LES case study.

2. Data and methods

2.1. Wind farm data

EnBW Baltic 1 (EB1) was by the time of commissioning the first commercial offshore wind farm in Germany. It is located about 16 km north of the Darß-Zingst peninsula within the southern Baltic Sea (Fig. 1(a)). The wind farm consists of 21 pitch-controlled Siemens (SWT-2.3-93) wind turbines, each with a rotor diameter of 93 m (1D), a hub height of 67 m (1H) and a rated power of 2.3 MW. The turbines are founded on monopiles in a water depth of around 18 m. The wind farm is arranged in a triangular shape (Fig. 1(b)) and therefore it allows for studying multiple wake situations for different wind directions. A SCADA dataset (power, nacelle position, nacelle wind speed, status; among others) of three full years (April 2011–March 2014) was available for this study. The data were filtered for downtimes, curtailments and other non-normal operation data. Afterwards, a power deficit for each turbine of the wind farm was calculated as

$$P_{def} = 1 - \frac{P_{wake}}{P_{free}} \quad (1)$$

with P_{def} the power deficit of each individual wind turbine, P_{wake} the measured power of the wind turbine and P_{free} the power of a reference turbine in the undisturbed flow. As reference turbines, the turbines at the corners of the wind farm were selected, depending on the wind direction. For a wind sector of 0°–120° turbine B01 was selected, for 120°–240° – B06 and for 240°–360° – B21. Wind speed measurements were obtained from the nacelle anemometers. The wind direction was derived from the nacelle position. Comparisons with data from a Light Detection And Ranging (LiDAR) campaign within the wind farm showed only small differences of the average nacelle positions as well as average wind speeds measured on top of the nacelle to the wind direction and wind speed derived from the LiDAR data.

2.2. LES framework

Simulations of the wind farm flow were conducted with the LES model PALM (A PArallelized LES Model) (Raasch and Schröter, 2001). The model uses a staggered Arakawa C-grid which is stretched in vertical direction above the top of the ABL. A fifth order advection scheme by Wicker and Skamarock (2002) was used. Subgrid fluxes were prescribed by the 1.5 order flux gradient subgrid closure scheme following Deardorff (1980). The boundary conditions were defined by a geostrophic wind speed (u_g,v_g), a roughness length (z_0) and a potential temperature profile. The Monin–Obhukhov similarity theory (MOST) was applied between the surface and the first computational grid level.

The simulation chain in this study consisted of pre-runs (PreRun1, PreRun2) without the effect of wind turbines in which the ABL was created and a subsequent main-run (MainRun) that was including the effect of the wind turbines. To initiate the development of turbulence, the pre-runs were initialized with random perturbations. Lateral and longitudinal cyclic boundary conditions were used (PreRun1,2). Afterwards, the actual wind farm simulation (MainRun) was driven by a turbulence recycling method in longitudinal flow direction (Kataoka and Mizuno, 2002). The inflow was realized by Dirichlet (fixed profile), the outflow by radiation boundary conditions. The model has been applied in SABLs in several studies (Beare et al., 2006; Steinfeld et al., 2007, among others).

To model the effect of wind turbines on the ABL, several wind turbine parametrizations of different complexity (based on Calaf et al., 2010; Mikkelsen, 2003; Wu and Porté-Agel, 2011) were adapted and implemented in the code. These parametrizations have been applied and verified in several research projects (e.g. Steinfeld et al., 2010; Witha et al., 2014a, b). The wind turbine model used in this study is described in more detail in Section 2.2.1. To include effects of the coastal discontinuity, a series of simulations was conducted employing the set-up described in Section 2.2.2.

2.2.1. Wind turbine parametrization

For a detailed but computationally efficient representation of the effect of the wind turbines on the flow, the LES model PALM was extended by an "enhanced actuator disk model with rotation" (ADM-R) (similar to the model used in Wu and Porté-Agel, 2011). Within this parametrization, the rotor disk is subdivided into rotor annulus segments on which the resulting lift and drag forces per segment are calculated independently from the actual position of a certain blade at the considered time instance. We are averaging the loads on each rotor annulus segment and project them afterwards onto the grid of the LES. A schematic illustration of the rotor representation in the ADM-R wind turbine parametrization is shown in Fig. 2.

This parametrization has the advantage that the time-step of the simulation is not determined by the rotational speed of the rotor blade but solely by the flow solver itself and is therefore

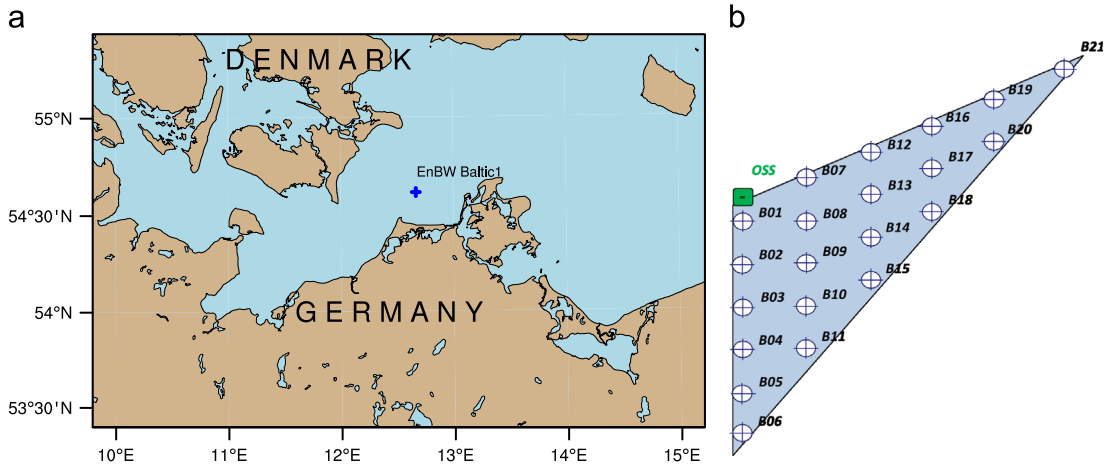

Fig. 1. Map of the Southern Baltic Sea region with the position of the offshore wind farm EnBW Baltic 1 (a), as well the layout of the wind farm with its 21 wind turbines and the offshore substation (OSS) inside the wind farm (b).

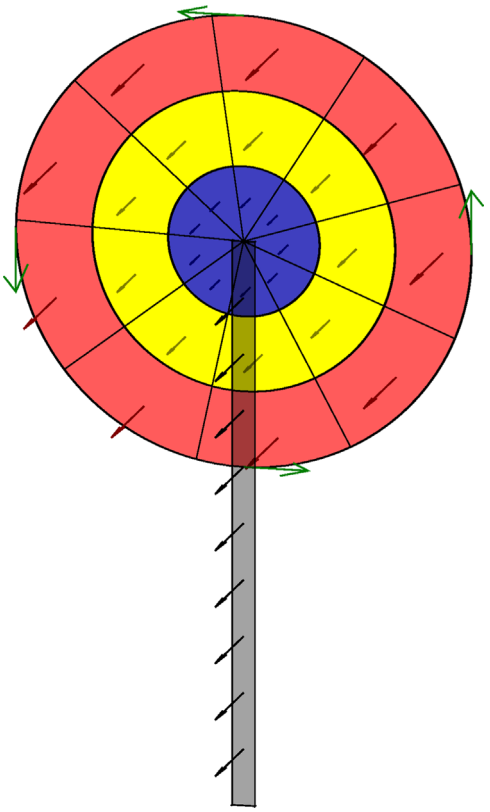

Fig. 2. Schematic illustration of the rotor representation in the ADM-R wind turbine parametrization. The rotor disk is subdivided into annulus ring segments on each of which the corresponding shares of lift and drag forces are calculated individually, indicated here by the arrows. The influence of tower and nacelle is represented by constant drag coefficients (see Eq. (9)).

about one order of magnitude faster than an actuator line parametrization, while keeping the details of the wake structure on averaged quantities (Witha et al., 2014a). Thus, the parametrization allows for detailed LES of wind farm flows. We assume rigid rotor blades which are rotating with constant rotational speed. The resulting forces per rotor annulus segment of span-wise length Δr are

$$f_L = \frac{1}{2}\rho_0 V_{rel}^2 c_L \frac{N_B c \Delta r}{2\pi r \Delta r} \tag{2}$$

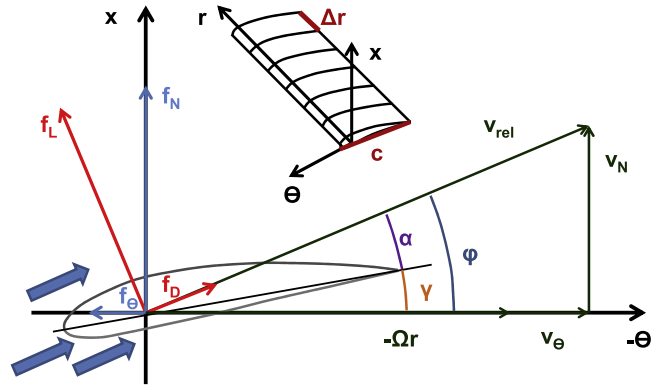

Fig. 3. Illustration of the forces on a blade element of a wind turbine (adapted from Porté-Agel et al., 2011).

$$f_D = \frac{1}{2}\rho_0 V_{rel}^2 c_D \frac{N_B c \Delta r}{2\pi r \Delta r} \tag{3}$$

with ρ_0 the density of the air, V_{rel} the relative velocity at the centre of the blade segment, c_L, c_D lift and drag coefficients of the rotor blade element depending on the angle of attack (α), respectively, N_B the number of blades, c the chord of the blade element and r the distance of the rotor blade element to the hub. An illustration of these forces on a blade element is shown in Fig. 3.

The resulting forces are afterwards projected onto the axial (f_N) and tangential (f_Θ) planes and inverted to represent the forces on the flow instead of the blade:

$$f_N = f_L \cos(\phi) + f_D \sin(\phi) \tag{4}$$

$$f_\Theta = f_L \sin(\phi) - f_D \cos(\phi) \tag{5}$$

where ϕ is the inflow angle between the rotor plane and the wind speed relative to the rotor blade (V_{rel}), calculated as

$$\phi = \tan^{-1}\left(\frac{V_N}{\Omega r - V_\Theta}\right) \tag{6}$$

with V_N the wind speed normal to the rotor plane and $\Omega r - V_\Theta$ the tangential wind speed component without the circular speed of the blade (see Fig. 3). Ω is the rotational speed of the wind turbine. Finally, these forces are interpolated onto the grid of the LES and smeared with a Gaussian kernel (η_ϵ):

$$\eta_\epsilon(d) = \frac{1}{\epsilon^3 \pi^{\frac{3}{2}}} \exp\left[-\left(\frac{d}{\epsilon}\right)^2\right] \tag{7}$$

with d the distance between an arbitrary grid point and the centre of an annulus segment, and ϵ the width of the smearing. This parameter is set to two times the grid spacing, which turned out to be a reasonable value (Troldborg et al., 2014). The actual force per angular segment applied to the grid points/volume elements arises from this smearing which is afterwards applied onto the flow:

$$\mathbf{f}_\epsilon(x,y,z) = \sum_{1<\beta<B_{seg}} (f_\Theta \mathbf{e}_\Theta + f_N \mathbf{e}_N)\eta_\epsilon(d_{b,r}(x,y,z)) \quad (8)$$

where the sum is calculated over the number of annulus segments (B_{seg}). The model is also capable of considering the tilt and yaw angle of the rotor. The influence of the tower as well as the nacelle are accounted for by

$$f_{[tow,nac]} = \frac{1}{2}\rho_0 V^2 c_{D[tow,nac]} \frac{D\Delta h}{Dh} \quad (9)$$

with $c_{D[tow,nac]}$ constant drag coefficients for the tower respectively nacelle from manufacturers specifications, D the diameters of the tower/nacelle and V the wind speed at the considered height h.

2.2.2. Simulation set-up

Due to the proximity of the wind farm to the shore, internal boundary layers that form during the coastal passage are an important feature of the Baltic Sea region. This impact was included in the simulations by the following procedure: first, the pre-run (PreRun1) with cyclic boundary conditions was carried out with a constant roughness length representing the land surface and constant potential temperature profile (neutral stratification) until a quasi-stationary state was achieved. In a second step, this simulation was continued with a reduction of the surface roughness length and surface temperature to the properties of the new surface (sea) (PreRun2 – see Table 1). The third simulation was the actual wind farm simulation, including the parametrized wind turbines (ADM-R) in non-cyclic lateral boundary conditions, using the inflow conditions from PreRun2 as input data.

In all three simulations, the resolution in all three spatial directions was 4 m inside the ABL. The value of the sea surface roughness length was taken from measurements at an offshore met mast within the Baltic Sea (FINO2) and corresponds to literature values for coastal areas (Stull, 1988, p. 380). The surface temperatures represent a typical late spring day in the region.

3. Results

3.1. Measured wake effects

Fig. 4(a) shows the average power deficit (Eq. (1)) as function of wind direction (hereafter wake rose) for the wind turbine B13 in the centre of the wind farm averaged over all atmospheric stability conditions (see Fig. 1(b)). The wake rose is plotted for the wind speed interval [4,10] m s^{-1} measured at the nacelle of the turbine, ensuring operating conditions below rated power.

The wake effects can be related to the distance of the surrounding wind turbines with the strongest wake effects on the north–south axis, where the distance to the upstream turbine is shortest with about 6D. Several non-waked sectors ($P_{Def} = 0$) can be identified for north-westerly and north-easterly winds. For a narrow south-easterly sector ($\approx 135^\circ$), a negative wake deficit (power excess) is obtained. The wind turbine in the centre of the wind farm (B13) is on average harvesting about 10% more power than the corresponding reference turbine for this sector (B06).

The power deficit for varying atmospheric stabilities is shown in Fig. 4(b). As stability parameter, the Bulk-Richardson number (Zoumakis and Kelessis, 1991) was calculated from operational analysis data from the COSMO-DE numerical weather prediction (NWP) model (Doms and Schättler, 2002) as

$$Ri_b = \frac{g}{\overline{\Theta}} \frac{\Delta\Theta/\Delta z}{(\Delta U/\Delta z)^2} \quad (10)$$

with g the gravitational constant, $\overline{\Theta}$ an average potential temperature, $\Delta\Theta$ the potential temperature and ΔU wind speed differences between two model levels and Δz the vertical distance between these model levels. Data from the COSMO-DE model levels 47 (122.32 m) and 49 (35.72 m) are selected at the grid point closest to the wind farm to characterize the stability conditions approximately across the rotor disk. A Bulk-Richardson number of $|Ri_b| < 0.15$ is defined as neutral (solid line), $Ri_b > 0.15$ as stable (dashed) and $Ri_b < -0.15$ as unstable (dotted).

It becomes apparent that the wake effect in the stably stratified situation is up to twice as strong as in the unstably stratified ABL. This finding is in agreement with the results of other studies where similar differences were reported (e.g. Hansen et al., 2012). This effect is most prominent in situations with long distances between the turbines, e.g. the north-eastern and south-western sectors, where the distance of the upstream turbines is more than 10D. The power excess for south-easterly winds is amplified in non-neutral stratification peaking with about P_{Def}=13% for a wind direction of 135°. It should be noted here that although a fixed wind speed interval is used, the average wind speed per direction bin can vary by up to 1 m s^{-1} in between the stability classes. The power excess for south-easterly winds are investigated in more detail by means of LES in the following subsection.

3.2. Simulated wake effects

To investigate the shown measured wake effects inside the wind farm EnBW Baltic 1 in more detail, a south-easterly incident flow is simulated. The distance of the wind farm to the coast in this direction is about 30 km. The average wind speeds at hub height are in the order of 9 m s^{-1} for this wind direction and stability. The model is therefore driven by a constant geostrophic wind speed of u=9.5 m s^{-1}, v=−4.2 m s^{-1}, establishing a horizontal wind speed at hub height of about 9 m s^{-1}. A capping inversion of $d\Theta/dz$ = 8 K/100 m is defined at a height of 500–600 m, which is a typical mixing layer height in the Baltic Sea region (Sempreviva and Gryning, 2000). After a 24 h neutrally stratified pre-run (PreRun1 in Table 1), a second pre-run (PreRun2) is following for a simulation time of another hour to obtain the actual sea fetch. Fig. 5 shows the development of the horizontal wind speed profile as well as the potential temperature after the coastal passage. The solid black profile shows the stationary neutral state at the end of the first pre-run. The dashed–dotted lines indicate the development of the profiles (10 min averages) within the first hour after changing the

Table 1
Simulation set-up for the wind farm simulation.

Name	Grid size	Simulation time (h)	Boundary conditions	Roughness length z_0 (m)	Surface temp. Θ (K)
Land-ABL (PreRun1)	768 × 768 × 192	24	Cyclic	0.4	293.15
Sea-ABL (PreRun2)	768 × 768 × 192	1	Cyclic	0.002	285.15
Wind farm (MainRun)	4096 × 2048 × 192	1	Turb. recycling	0.002	285.15

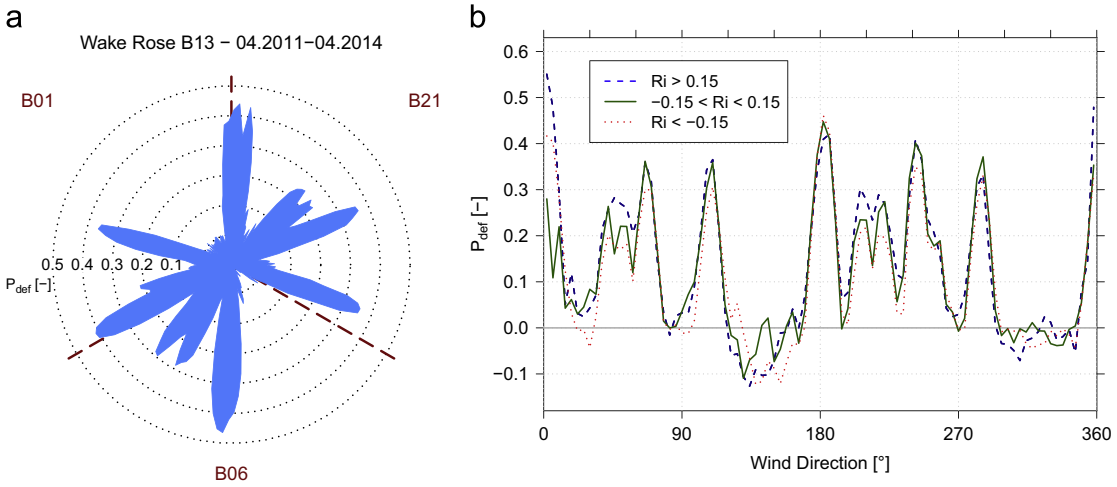

Fig. 4. Non-dimensional power deficit P_{def} (Eq. (1)) from SCADA data for the wind turbine B13 in the centre of the EB1 wind farm as circular plot for all atmospheric stabilities (a) and subdivided by a Richardson criterion into stable, neutral and unstable stratification (b).

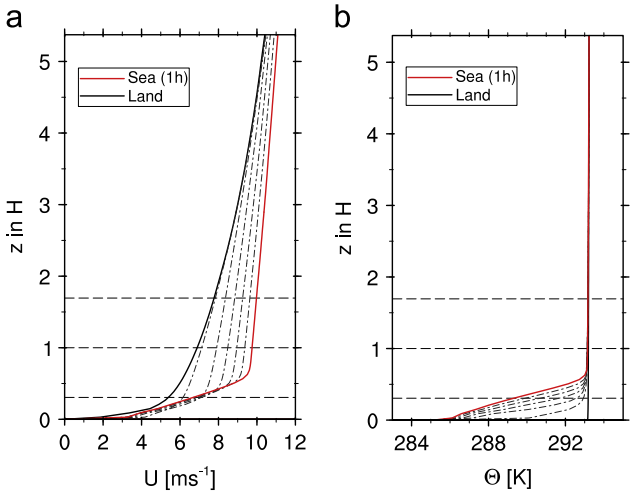

Fig. 5. Vertical profiles (10 min averages) of horizontal wind speed (a) and potential temperature (b) as function of time obtained from the pre-runs. The bold black lines mark the quasi-stationary neutrally stratified state at the end of PreRun1, the dashed–dotted lines the evolution of the profiles within the first hour after the coastal passage (in PreRun2), the (red) bold rightmost line in (a) and the (red) bold leftmost line in (b) the inflow profile for the main run.

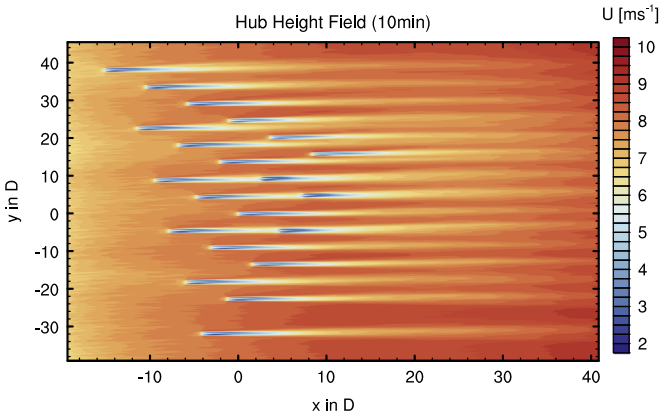

Fig. 6. Hub height wind field obtained from LES (MainRun) with the ADM-R wind turbine parametrization, averaged over 10 min. The wind farm is turned by 135° to the north in clockwise direction.

surface properties. Due to the reduced friction, the wind speeds are continuously increasing especially at the height of the rotor disk (dashed horizontal lines). The cooling of the ABL induced by the lower temperature of the sea surface leads to a development of an SABL. This cooling propagates vertically up to a height of about 0.5H within the first hour after the coastal passage. The red solid lines in Fig. 5 show the corresponding wind speed and temperature profiles at the end of PreRun2 which is used within the simulation chain as inflow conditions for the wind farm simulation. For the actual wind farm simulation (MainRun in Table 1) the wind farm is turned by 135°, to allow for non-cyclic conditions in longitudinal and cyclic conditions in lateral flow direction. Fig. 6 shows a section of the hub height wind field averaged over 10 min obtained from the main-run. The wind farm is centred around the wind turbine B13 ($x=0D$, $y=0D$), the turbine for which the power deficits are shown in Fig. 4. The wakes of all 21 wind turbines are in evidence.

In addition, a general increase of the wind speed with downstream distance from the coast is visible, as shown in Fig. 6. This increase is due to the sudden change of surface roughness and temperature. In heights of several tens of meters, the flow transits from a force balance of Coriolis, friction and pressure gradient force to a balance of Coriolis and pressure gradient force only. This leads to an oscillation of the wind vector and thus a development of a low-level jet later (Emeis, 2013). This is likely one part of the explanation for the speed-up described in Section 3.1. The reference turbine (B06, leftmost, in flow direction, turbine in Fig. 6) is for this wind direction sector about 2 km closer to the coast and thus encountering lower wind speeds than the turbine B13. This is also confirmed when comparing the south-easterly to the north-westerly sector (in Fig. 4), where a negative power deficit is not observed. The other part of the explanation is a speed-up due to the nozzle flow between the surrounding turbines (mostly B14 and B18). This effect can also be observed in Fig. 7, which shows a detail of the horizontal wind field shown in Fig. 6. Between the turbines local jets of high wind speed form. In the jet cores these wind speeds can be more than 10% higher than the wind farm inflow.

In Fig. 8 the average turbulence intensity of all three components at hub height obtained from MainRun is presented. Due to the development of an SABL, the turbulence tends to reduce with increasing fetch. The impact of the wind turbines on the flow can clearly be observed by an increase in turbulence intensity up to 25%. The largest turbulence intensities can be found downstream of the second turbine, when the downstream turbine is located in a full wake situation. For the simulated inflow (135°), there are three turbines only that are directly aligned with an upstream

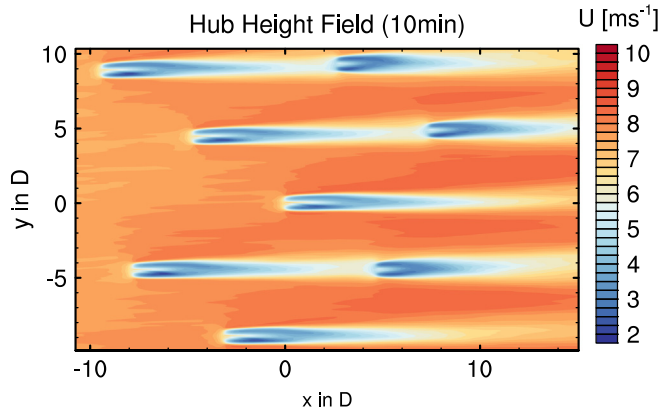

Fig. 7. Section of hub height wind field obtained from LES (MainRun) with the ADM-R wind turbine parametrization, averaged over 10 min.

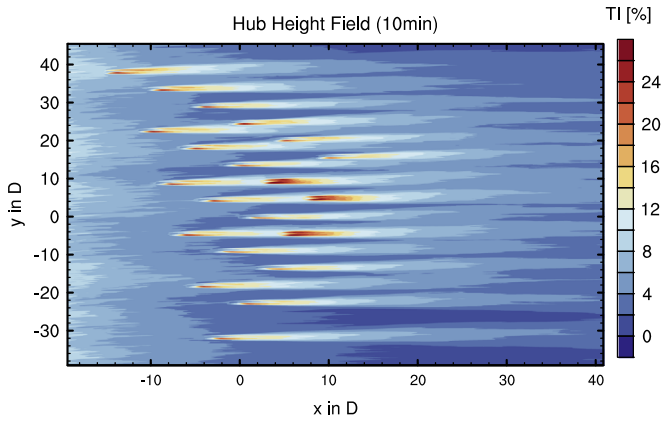

Fig. 8. Hub height field of turbulence intensity (all three components) obtained from LES (MainRun), averaged over 10 min. The wind farm is turned by 135° to the north in clockwise direction.

turbine and thus yielding to turbulence intensities above 20%. The hub height fields show a slight deviation of the wakes towards the left in flow direction. This deflection is likely due to the increased friction by the wind turbines and thus a decreasing importance of Coriolis force.

In the following section the flow around the B13 wind turbine will be investigated in more detail. Figs. 9–11 show along-wind vertical cross sections through the wake centre of the wind turbine B13 obtained from MainRun. The instantaneous (a) and average (b) horizontal wind speed in Fig. 9 indicate the impact of the turbines on the flow in more detail. The wake shows two distinct maxima with the wake cores at about two-third of the rotor radius. Due to the strong vertical wind speed gradient in the inflow, the wake is deflected vertically. The flow is compressed below the rotor disk so that the wind speed increases there. Upstream of the rotor, an area of reduced velocity due to the blocking caused by the rotor disk can be found up to a distance of about $-1D$. The instantaneous velocity field (Fig. 9(a)) shows strong wind speed gradients at the edge of the wake. These gradients are specifically strong in a distance of 8–12D, a typical spacing of wind turbines in offshore wind farms. The vertical along-wind potential temperature field is presented in Fig. 10. The instantaneous field (a) shows that the temperature fluctuations are vertically amplified by the mixing of the rotor. While the temperature field is homogeneous above a height of around 1H upstream of the rotor disk, the rotor induced turbulence mixes high temperatures down and low temperatures up. This can also be observed in the average temperature field (b), where the temperature gradient behind the rotor is generally reduced compared to the situation upstream of the rotor.

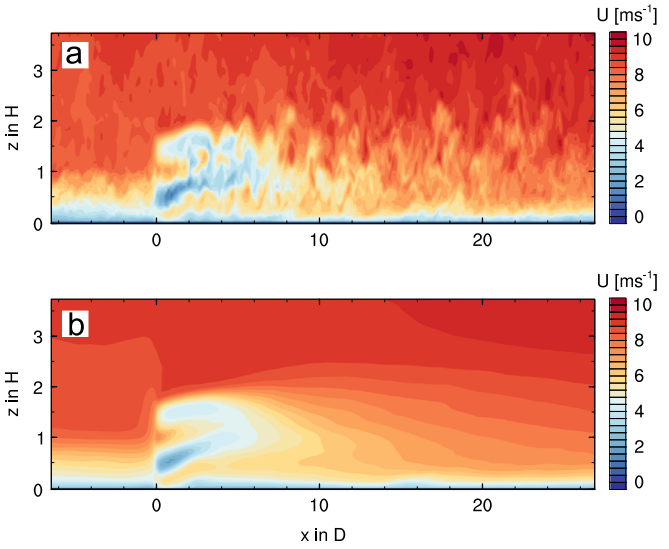

Fig. 9. Along-wind vertical cross-section of instantaneous (a) and average (b) horizontal wind speed through the centre of the wake of the wind turbine B13 from LES (MainRun).

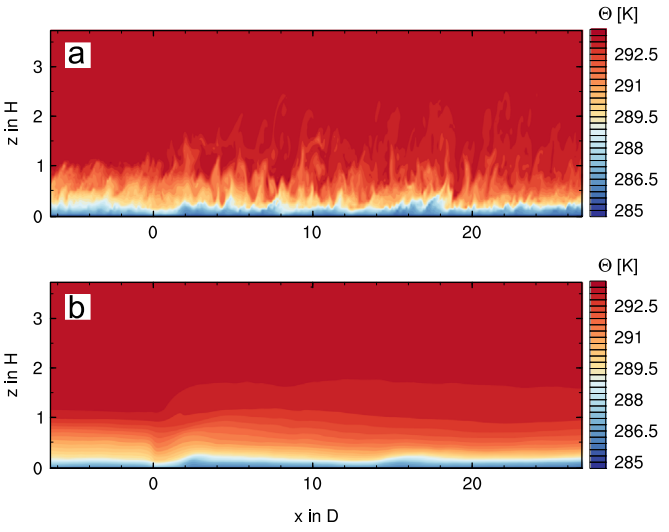

Fig. 10. Along-wind vertical cross-section of instantaneous (a) and average (b) potential temperature through the centre of the wake of the wind turbine B13 from LES (MainRun).

Consequently, the turbine-induced mixing tends to neutralize the stratification. In a downstream distance of around 1D a vertical transport of low temperatures from the sea surface to higher altitudes can be found. This “bump” in the potential temperature field coincides with the undercurrent of the rotor disk shown in the wind field (Fig. 9). Average turbulent quantities of the along-wind vertical flow are presented in Fig. 11 with the average vertical kinematic heat flux (a) and the average turbulence intensity (of all three components) (b). It can be seen that the turbines amplify the negative heat flux from atmosphere towards the sea surface. This is especially true in a distance of 2–10D and in the lower part of the rotor disk. The negative kinematic heat flux is caused by the turning of the wake. In the upper part of the rotor disk and in a downstream distance of up to 4D a small area of positive vertical heat flux can be found. The counter-clockwise turning of the flow as counterpart to the clockwise turning of the rotor thus accounts for the patterns in the vertical heat flux. The vertical field of turbulence intensity shows that the highest turbulence occurs at about the lower tip of the rotor. This area coincides with the highest inflow wind speed

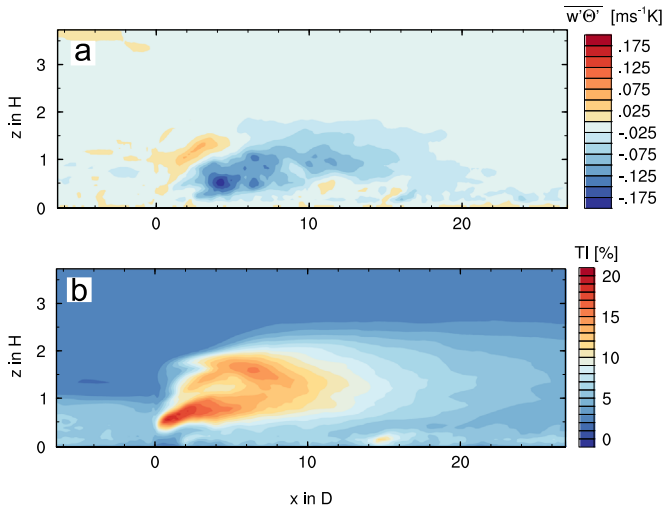

Fig. 11. Along-wind vertical cross-section of time averaged vertical kinematic heat flux (a) and turbulence intensity (of all three components) (b) through the centre of the wake of the wind turbine B13 from LES (MainRun).

gradient (Fig. 9(b)). Abipolar wake structure can be found in the turbulence intensity cross-section up to a distance of about 8*D*. The turbulence intensity reaches upstream values in the lower part of the rotor after about 25*D*, whereas the low inflow turbulence intensities of 2–3% in the upper part of the rotor disk are deflected by the turbine to altitudes of 2.5*H*.

4. Discussion and conclusions

Within this study we investigated measured and simulated wind farm wake effects in marine boundary layers. A three-year dataset of operational wind farm data was analysed and classified by means of thermal stratification. An undisturbed stability time series at the wind farm location was not available. Therefore, a dataset from the NWP model COSMO-DE was used and wake deficits from this dataset are calculated. Generally NWP models tend to underestimate SABLs mainly due to an artificially increased diffusion, which generally improves the forecast quality of the large-scale flow and near-surface temperatures (Sandu et al., 2013). Nevertheless, the classification showed typical results obtained in similar studies (e.g. Hansen et al., 2012; Wharton and Lundquist, 2012).

In an SABL the wake effects were stronger than in neutral and unstable stratification especially for distances to the upstream turbines of more than 10*D*. A possible explanation for the enhanced wake effects is that the momentum fluxes which act in refilling the wake are decreasing with increasing stability (Emeis, 2013). To investigate the wake effects by wind direction the dataset was binned into wind direction, stability and wind-speed bins. The dataset showed that long-term time series of several years are needed to give clear statements. A wind direction sector of around 20° for which the investigated turbine was located at the centre of the wind farm a power excess compared to the reference turbine is observed.

This phenomenon was investigated by means of LES, including a land–sea passage of a neutrally stratified stationary ABL with typical land-surface properties (high roughness length) onto a sea surface (lower roughness and surface temperature). In a third step the wind farm was included into the simulation chain with an enhanced actuator disk parametrization including rotational effects. The simulations showed that the distance of the wind farm to the coast is a crucial factor for the power output of the wind turbines inside the farm. An SABL forms after the coastal passage which is still under development with an increasing mean wind speed across the wind farm. Thus, one main reason for the power excess of the turbine in the wind farm centre is the fact that the reference turbine at the edge of the wind farm was about 2 km closer to the coast and thus affected by a lower average wind speed. Another important factor is that the wind farm flow is dominated by strong horizontal and vertical wind speed gradients. This is especially true inside the wind farm, where local horizontal areas of high wind speeds due to the blocking of the turbines form. A more detailed investigation of a wind turbine wake in the centre of the wind farm showed that the turbines generally tend to reduce the stability and therefore neutralize the ABL due to the mixing induced by the rotors. The strong vertical gradient in temperature and horizontal wind speed is decreased, while the (negative) kinematic heat flux is generally intensified. Turbulence levels downstream of the rotor are strongly enhanced and do not reach the inflow conditions within 25*D*.

These results generally show the importance of enhanced wind turbine parametrizations which account for non-uniform loading and rotation. A validation of the numerical results with measured data from the wind farm is a challenging task: due to insufficient computational power, wind-farm LES can be employed for case studies only. This requires long-term measurement data and a thorough filtering of these data to obtain similar boundary conditions. First steps towards a validation of our model with other models and data have been made. In addition we are participating in the “IEA Task 31: Benchmarking of wind farm flow models” (IEA Wind, 2014).

In the framework of the research project in which this study is carried out, we are currently working on including the shown results into wind farm control strategies as well as wind power forecast models. In the future, a more detailed numerical investigation of properties of stable and unstable boundary layers (e.g. low level jets and roll convection) and their interaction with wind turbines and wind farms is planned.

Acknowledgements

The work presented in this study is funded by the National Research Projects “Baltic I” and “Parallelrechner-Cluster für CFD und WEA-Modellierung” (FKZ 0325215A and 0325220; Federal Ministry for Economic Affairs and Energy) and the Ministry for Education, Science and Culture of Lower Saxony. Computer resources have been partly provided by the North German Supercomputing Alliance (HLRN). We thank Deutscher Wetterdienst (DWD) for providing analysis data.

References

Aitken, M.L., Kosović, B., Mirocha, J.D., Lundquist, J.K., 2014. Large eddy simulation of wind turbine wake dynamics in the stable boundary layer using the weather research and forecasting model. J. Renew. Sustain. Energy 6, 033137. http://dx.doi.org/10.1063/1.4885111.

Barthelmie, R., Frandsen, S., Rethore, P., Jensen, L., 2007. Analysis of atmospheric impacts on the development of wind turbine wakes at the Nysted wind farm. In: European Offshore Wind Conference 2007, Berlin, Germany.

Beare, R.J., Macvean, M.K., Holtslag, A.A., Cuxart, J., Esau, I., Golaz, J.C., Jimenez, M.A., Khairoutdinov, M., Kosovic, B., Lewellen, D., et al., 2006. An intercomparison of large-eddy simulations of the stable boundary layer. Bound.-Layer Meteorol. 118, 247–272. http://dx.doi.org/10.1007/s10546-004-2820-6.

Calaf, M., Meneveau, C., Meyers, J., 2010. Large eddy simulation study of fully developed wind-turbine array boundary layers. Phys. Fluids, 22. http://dx.doi.org/10.1063/1.3291077.

Churchfield, M.J., Lee, S., Moriarty, P.J., Martinez, L.A., Leonardi, S., Vijayakumar, G., Brasseur, J.G., 2012. A large-eddy simulation of wind-plant aerodynamics. 50th AIAA Aerospace Sciences Meeting, Nashville, Tennessee, January 9–12, 2012.

Deardorff, J.W., 1980. Stratocumulus-capped mixed layers derived from a three-dimensional model. Bound.-Layer Meteorol. 18, 495–527. http://dx.doi.org/10.1007/BF00119502.

Doms, G., Schättler, U., 2002. A Description of the Nonhydrostatic Regional Model LM. Technical Report. Deutscher Wetterdienst, 140 pp.

Dörenkämper, M., Tambke, J., Steinfeld, G., Heinemann, D., Kühn, M., 2014. Atmospheric impacts on power curves of multi-megawatt offshore wind turbines. In: Proceedings of the Science of Making Torque from Wind J. Phys.: Conf. Ser. 555:0122029, http://dx.doi.org/10.1088/1742-6596/555/1/012029.

El Kasmi, A., Masson, C., 2008. An extended k–ε model for turbulent flow through horizontal-axis wind turbines. J. Wind Eng. Ind. Aerodyn. 96, 103–122. http://dx.doi.org/10.1016/j.jweia.2007.03.007.

Emeis, S., 2010. A simple analytical wind park model considering atmospheric stability. Wind Energy 13, 459–469. http://dx.doi.org/10.1002/we.367.

Emeis, S., 2013. Wind Energy Meteorology: Atmospheric Physics for Wind Power Generation Springer, Berlin Heidelberg, 198.

EWEA, 2014. The European Offshore Wind Industry—Key Trends and Statistics 2013. Technical Report. European Wind Energy Association, 22 pp.

Hansen, K.S., Barthelmie, R.J., Jensen, L.E., Sommer, A., 2012. The impact of turbulence intensity and atmospheric stability on power deficits due to wind turbine wakes at Horns Rev wind farm. Wind Energy 15, 183–196. http://dx.doi.org/10.1002/we.512.

IEA Wind, 2014. International Energy Agency, Task 31: Benchmarking of Wind Farm Flow Models. URL ⟨http://www.ieawind.org/task_31.html⟩.

Jimenez, A., Crespo, A., Migoya, E., Garcia, J., 2007. Advances in large-eddy simulation of a wind turbine wake. J. Phys. Conf. Ser. 75, 012041. http://dx.doi.org/10.1088/1742-6596/75/1/012041.

Kataoka, H., Mizuno, M., 2002. Numerical flow computation around aeroelastic 3D square cylinder using inflow turbulence. Wind Struct. Int. J. 5, 379–392. http://dx.doi.org/10.12989/was.2002.5.2_3_4.379.

Mikkelsen, R., 2003. Actuator Disc Methods Applied to Wind Turbines (Ph.D. thesis). Technical University of Denmark.

Mirocha, J., Kosovic, B., Aitken, M., Lundquist, J., 2014. Implementation of a generalized actuator disk wind turbine model into the weather research and forecasting model for large-eddy simulation applications. J. Renew. Sustain. Energy 6, 013104. http://dx.doi.org/10.1063/1.4861061.

Porté-Agel, F., Wu, Y.T., Chen, C.H., 2013. A numerical study of the effects of wind direction on turbine wakes and power losses in a large wind farm. Energies 6, 5297–5313. http://dx.doi.org/10.3390/en6105297.

Porté-Agel, F., Wu, Y.T., Lu, H., Conzemius, R.J., 2011. Large-eddy simulation of atmospheric boundary layer flow through wind turbines and wind farms. J. Wind Eng. Ind. Aerodyn. 99, 154–168. http://dx.doi.org/10.1016/j.jweia.2011.01.011.

Raasch, S., Schröter, M., 2001. PALM—a large-eddy simulation model performing on massively parallel computers. Meteorol. Z. 10, 363–372. http://dx.doi.org/10.1127/0941-2948/2001/0010-0363.

Sandu, I., Beljaars, A., Bechtold, P., Mauritsen, T., Balsamo, G., 2013. Why is it so difficult to represent stably stratified conditions in numerical weather prediction (NWP) models? J. Adv. Model. Earth Syst. 5, 117–133. http://dx.doi.org/10.1002/jame.20013.

Sathe, A., Gryning, S.E., Peña, A., 2011. Comparison of the atmospheric stability and wind profiles at two wind farm sites over a long marine fetch in the North Sea. Wind Energy 14, 767–780. http://dx.doi.org/10.1002/we.456.

Sempreviva, A.M., Gryning, S.E., 2000. Mixing height over water and its role on the correlation between temperature and humidity fluctuations in the unstable surface layer. Bound.-Layer Meteorol. 97, 273–291. http://dx.doi.org/10.1023/A:1002749729856.

Smedman, A.S., Bergström, H., Grisogono, B., 1997. Evolution of stable internal boundary layers over a cold sea. J. Geophys. Res.—Oceans 102, 1091–1099. http://dx.doi.org/10.1029/96JC02782.

Smedman, A.S., Högström, U., Bergström, H., 1996. Low level jets—a decisive factor for offshore wind energy siting in the Baltic Sea. Wind Eng. 20, 137–147.

Sørensen, J.N., Shen, W.Z., 2002. Numerical modeling of wind turbine wakes. J. Fluids Eng. 124, 393–399. http://dx.doi.org/10.1115/1.1471361.

Steinfeld, G., Letzel, M.O., Raasch, S., Kanda, M., Inagaki, A., 2007. Spatial representativeness of single tower measurements and the imbalance problem with eddy-covariance fluxes: results of a large-eddy simulation study. Bound.-Layer Meteorol. 123, 77–98. http://dx.doi.org/10.1007/s10546-006-9133-x.

Steinfeld, G., Tambke, J., Peinke, J., Heinemann, D., 2010. Development of a tool for the study of flow conditions and turbulent loads in offshore wind farms. In: Proceedings of the European Wind Energy Conference (EWEC) 2010, Warsaw, Poland.

Stull, R.B., 1988. An introduction to boundary layer meteorology, Kluwer Academic Publishers, Dordrecht, 666.

Troldborg, N., Sorensen, J.N., Mikkelsen, R., Sorensen, N.N., 2014. A simple atmospheric boundary layer model applied to large eddy simulations of wind turbine wakes. Wind Energy 17, 657–669. http://dx.doi.org/10.1002/we.1608.

Wharton, S., Lundquist, J., 2010. Atmospheric stability impacts on power curves of tall wind turbines—an analysis of a west coast North American wind farm. Technical Report, LLNL-TR-424425. Lawrence Livermore National Laboratory (LLNL).

Wharton, S., Lundquist, J.K., 2012. Atmospheric stability affects wind turbine power collection. Environ. Res. Lett. 7, 014005. http://dx.doi.org/10.1088/1748-9326/7/1/014005.

Wicker, L.J., Skamarock, W.C., 2002. Time-splitting methods for elastic models using forward time schemes. Mon. Weather Rev. 130, 2088–2097 http://dx.doi.org/10.1175/1520-0493(2002)130 < 2088:TSMFEM > 2.0.CO;2.

Witha, B., Steinfeld, G., Heinemann, D., 2014a. Advanced turbine parameterizations in offshore les wake simulations, in: Extended abstract of the 6th International Symposium on Computational Wind Engineering (CWE) 2014, Hamburg, Germany.

Witha, B., Steinfeld, G., Dörenkämper, M., Heinemann, D., 2014b. Large-eddy simulation of multiple wakes in offshore wind farms, J. Phys.: Conf. Ser. 55:012108, http://dx.doi.org/10.1088/1742-6596/555/1/012108.

Wu, Y.T., Porté-Agel, F., 2011. Large-eddy simulation of wind-turbine wakes: evaluation of turbine parametrisations. Bound.-Layer Meteorol. 138, 345–366. http://dx.doi.org/10.1007/s10546-010-9569-x.

Zoumakis, N., Kelessis, A., 1991. The dependence of the bulk Richardson number on stability in the surface layer. Bound.-Layer Meteorol. 57, 407–414. http://dx.doi.org/10.1007/BF00120057.